3. Atmospheric model (MRI-AGCM3)

The atmospheric component (including land and ocean surfaces) model, MRI-AGCM3, was developed from a model by Mizuta et al. (2006) by the addition of a number of physical parameterization options and improvements, summarized in Table 1. The dynamics framework of MRI-AGCM3, which Mizuta et al. (2006) did not document in detail, is described in Section 3.1. In the subsequent sections, the major physical parameterizations developed for MRI-AGCM3 are described: cumulus convection (Section 3.2), radiation (Section 3.3), cloud model (Section 3.4), PBL (Section 3.5), land-surface model (Section 3.6), ocean surface processes (Section 3.7), and river–lake model (Section 3.8). Other components of MRI-AGCM3 are basically the same as in the original model of Mizuta et al. (2006).

3.1. Dynamics framework

In the MRI-AGCM3 global spectral atmospheric model, hydrostatic primitive equations are used as prognostic equations. A two-time-level semi-implicit semi-Lagrangian scheme is used for time integration. This scheme permits a longer time-step than the formerly used semi-implicit Eulerian scheme and realizes high efficiency. The vertically conservative semi-Lagrangian advection scheme is also globally conservative and therefore suitable not only for short-term weather predictions but also for long-time-period integrations such as experiments for projecting climate change.

The prognostic equations are given in Section 3.1.1, the vertically conservative semi-Lagrangian scheme is explained in Section 3.1.2, and the time integration scheme is described in Section 3.1.3.

3.1.1. Prognostic equations

The following hydrostatic primitive equations are used as prognostic equations.

$$\frac{\partial}{\partial t}\left(\frac{\partial p}{\partial \eta}\right) + \nabla \cdot \left(\mathbf{v}_H \frac{\partial p}{\partial \eta}\right) + \frac{\partial}{\partial \eta}\left(\dot{\eta} \frac{\partial p}{\partial \eta}\right) = 0 \tag{3.1}$$

$$\frac{dq}{dt} \equiv \frac{\partial}{\partial t}q + \mathbf{v}_H \cdot \nabla q + \dot{\eta}\frac{\partial}{\partial \eta}q = P_q \tag{3.2}$$

$$\frac{dT}{dt} = F_T + P_T + K_T \tag{3.3}$$

Table 1. List of MRI-AGCM3 options

Scheme/Model	Option name	References
Dynamics	1. Euler (obsolete)	JMA (2002)
	2. Semi-Lagrange	Section 3.1
Cumulus convection	1. AS type	Section 3.2.1, JMA (2002)
	2. Yoshimura	Section 3.2.2
	3. KF type	Section 3.2.3
Radiation	1. Shibata	Shibata and Aoki (1989) Shibata and Uchiyama (1992)
	2. JMA2004R1	Section 3.3
Cloud	1. Smith	Smith (1990)
	2. Tiedtke	Tiedtke (1993)
	3. MRI-TMBC	Section 3.4
PBL	1. Mellor-Yamada	Section 3.5.1 Mellor and Yamada (1974, 1982)
	2. MYNN	Section 3.5.2 Nakanishi (2001), Nakanishi and Niino (2004)
	3. Non-local	Section 3.5.3 Troen and Mahrt (1986), Holtslag and Boville (1993).
Land surface	1. JMA/SiB	Sellers et al. (1986), Sato et al. (1989)
	2. SiB0109	Hirai et al. (2007)
	3. HAL	Section 3.6
Ocean surface	1. JMA	JMA (2002)
	2. MRI	Section 3.7
River and lake	0. OFF	N/A
	1. GRiveT	Section 3.8
Gravity wave drag	1. Iwasaki	Iwasaki et al. (1989)
	2. Hines (experimental)	Hines (1997)
Terrestrial carbon cycle	1. Obata_2007	Obata (2007)
	2. Obata_2010	Section 8.1

$$F_T \equiv \frac{\kappa T_v \omega}{\left[1+\left(c_{pv}/c_{pd}-1\right)q\right]p} \tag{3.3a}$$

$$\frac{d\left(\mathbf{v}_H+2\mathbf{\Omega}\times\mathbf{r}\right)}{dt}=\mathbf{F}_{\mathbf{v}_H}+\mathbf{P}_{\mathbf{v}_H}+\mathbf{K}_{\mathbf{v}_H} \tag{3.4}$$

$$\mathbf{F}_{\mathbf{v}_H} \equiv -\nabla\Phi - R_d T_v \nabla \ln p \tag{3.4a}$$

$$\frac{\partial\Phi}{\partial\eta}=-\frac{R_d T_v}{p}\frac{\partial p}{\partial\eta} \tag{3.5}$$

$$T_v \equiv T\left\{1+\left(\frac{R_v}{R_d}-1\right)q\right\}. \tag{3.6}$$

Here, the following notations are used.

t : Time

p : Pressure

p_s : Surface pressure

η : Hybrid $p-\sigma$ vertical coordinate ($\sigma\equiv p/p_s$)

$\dot{\eta}$: $\dot{\eta}\equiv d\eta/dt$

$\mathbf{v}_H$: Horizontal wind

q : Water vapor mixing ratio

T : Temperature

T_v : Virtual temperature

R_d : Gas constant of dry air

R_v : Gas constant of water vapor

c_{pd} : Specific heat of dry air at constant pressure

c_{pv} : Specific heat of water vapor at constant pressure

ω : Vertical pressure at p coordinate, $\omega\equiv dp/dt$

κ : $\kappa\equiv R_d/c_{pd}$

F_T : Heating by adiabatic compression (expansion)

$\mathbf{F}_{\mathbf{v}_H}$: Pressure gradient force

$P_q, P_T, \mathbf{P}_{\mathbf{v}_H}$: Contribution by physical processes

$K_T, \mathbf{K}_{\mathbf{v}_H}$: Horizontal viscosity

$\mathbf{\Omega}$: Angular velocity of the rotation of the earth

  r   : Position vector from the center of the earth

  ∇ : Horizontal gradient on the η surface.

The η coordinate is a hybrid vertical coordinate that steadily changes from the terrain following σ coordinate near the surface to the p coordinate near the top (Simmons and Burridge, 1981). $\eta = \eta(p, p_s)$ is a monotonic function of p that satisfies $\eta(0, p_s) = 0$ and $\eta(p_s, p_s) = 1$. p can be defined as a function of η and p_s, and $A(\eta)$ and $B(\eta)$ are introduced to satisfy

$$p(\eta, p_s) = A(\eta) + B(\eta) \cdot p_s. \tag{3.7}$$

$A(\eta) = 0$ is satisfied in the lower layers near the surface (σ-coordinate), and $B(\eta) = 0$ is satisfied in the upper layers (p-coordinate).

3.1.2. Advection with a vertically conservative semi-Lagrangian scheme

The vertically conservative semi-Lagrangian scheme (briefly described by Yoshimura and Matsumura, 2003, 2005) is used for the advection calculation. The equation

$$\frac{\partial}{\partial t} q + \mathbf{v}_H \cdot \nabla q + \dot{\eta} \frac{\partial}{\partial \eta} q = 0 \tag{3.8}$$

is used to explain the calculation of the advection of q. Equation (3.8) is the same as Eq. (3.2) except that the right-hand side of Eq. (3.8) is 0 to simplify its explanation. The advection of T and $\mathbf{v}_H$, Eqs. (3.3) and (3.4), is calculated in basically the same way as that of q. From Eqs. (3.1) and (3.8),

$$\frac{\partial}{\partial t}\left(\frac{\partial p}{\partial \eta} q\right) + \nabla \cdot \left(\mathbf{v}_H \frac{\partial p}{\partial \eta} q\right) + \frac{\partial}{\partial \eta}\left(\dot{\eta} \frac{\partial p}{\partial \eta} q\right) = 0 \tag{3.9}$$

is derived, which is the conservation equation of water vapor. When $q = 1$, Eq. (3.9) is the same as Eq. (3.1), the mass conservation equation. From Eqs. (3.1) and (3.9),

$$\frac{d_H}{dt}\left(\frac{\partial p}{\partial \eta}\right) = -D \frac{\partial p}{\partial \eta} - \frac{\partial}{\partial \eta}\left(\dot{\eta} \frac{\partial p}{\partial \eta}\right) \tag{3.10}$$

$$\frac{d_H}{dt}\left(\frac{\partial p}{\partial \eta} q\right) = -D \frac{\partial p}{\partial \eta} q - \frac{\partial}{\partial \eta}\left(\dot{\eta} \frac{\partial p}{\partial \eta} q\right) \tag{3.11}$$

are derived, where $d_H/dt \equiv \partial/\partial t + \mathbf{v}_H \cdot \nabla$ represents horizontal advection and $D \equiv \nabla \cdot \mathbf{v}_H$ represents horizontal divergence.

Equations (3.10) and (3.11) are vertically discretized. There are K full levels in the vertical direction

and $\mathbf{v}_H, T, q$ are positioned at each full level ($k = 1, 2, 3, ..., K$). η is positioned at the half levels ($k = 1/2, 3/2, 5/2, ..., K + 1/2$), which are the boundaries between the full levels. At the lower boundary ($k = 1/2$), $p = p_s$, $\eta = 1$, and $\dot{\eta} = 0$ are satisfied. At the upper boundary ($k = K + 1/2$), $p = 0$, $\eta = 0$, and $\dot{\eta} = 0$ are satisfied. From Eq. (3.7), the pressure at the half level is obtained by

$$p_{k-1/2} = A_{k-1/2} + B_{k-1/2} p_s. \tag{3.12}$$

Equations (10) and (11) are vertically discretized (integrated from $k + 1/2$ to $k - 1/2$) as

$$\frac{d_H}{dt}(\Delta p_k) = -D_k \Delta p_k - \left(\dot{\eta}\frac{\partial p}{\partial \eta}\right)_{k-1/2} + \left(\dot{\eta}\frac{\partial p}{\partial \eta}\right)_{k+1/2} \tag{3.13}$$

$$\frac{d_H}{dt}(\Delta p_k q_k) = -D_k \Delta p_k q_k - \left(\dot{\eta}\frac{\partial p}{\partial \eta}q\right)_{k-1/2} + \left(\dot{\eta}\frac{\partial p}{\partial \eta}q\right)_{k+1/2}, \tag{3.14}$$

where Δp_k is defined as

$$\Delta p_k \equiv p_{k-1/2} - p_{k+1/2}. \tag{3.15}$$

The left-hand sides of Eqs. (3.13) and (3.14) represent horizontal advection, the first terms on the right-hand sides represent horizontal divergence (convergence), and the second and third terms on the right-hand sides represent vertical flux.
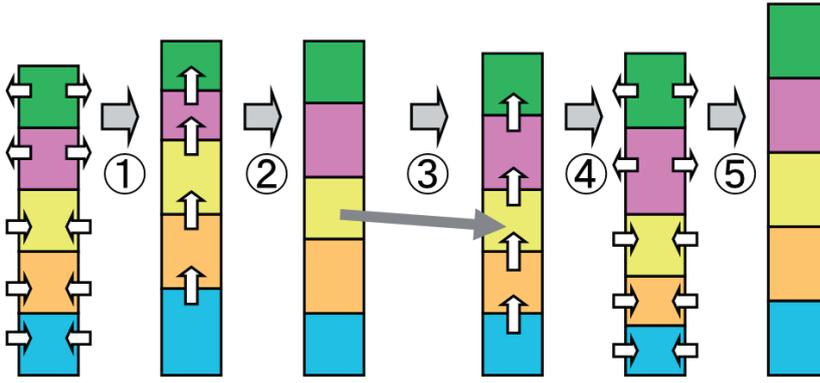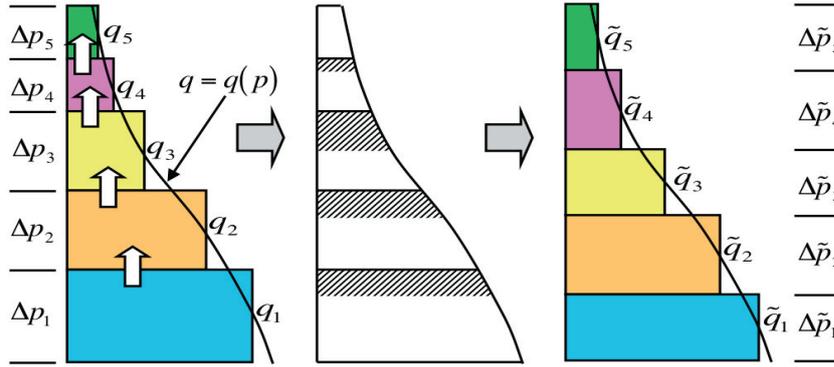
Three-dimensional advection is calculated by executing the time integration of these equations in the following order:

① Horizontal divergence

② Vertical flux

③ Horizontal advection

④ Vertical flux

⑤ Horizontal divergence.

Figure 2 shows the change in Δp_k due to the time integration of Eq. (3.13). The vertical flux (steps ② and ④) is calculated by the conservative semi-Lagrangian scheme. Figure 3 shows changes in Δp_k and q_k due to the vertical flux. The diagram on the left shows Δp_k and q_k before the vertical flux calculation. The distribution of $q = q(p)$ is obtained from q_k, which satisfies

$$\int_{p_{k+1/2}}^{p_{k-1/2}} q(p)dp = q_k \Delta p_k. \tag{3.16}$$

The hatched part of the diagram in the center of Fig. 3 represents q moving to the upper layer. The values of $\Delta \tilde{p}_k$ and $\tilde{q}_k$ after the vertical flux calculation are shown in the right diagram. $\tilde{q}_k$ is calculated as

Figure 2 Change of Δp_k due to time integration in one time step

Figure 3 Change of Δp_k and q before and after vertical flux calculation

$$\tilde{q}_k = \frac{1}{\Delta \tilde{p}_k} \int_{\tilde{p}_{k+1/2}}^{\tilde{p}_{k-1/2}} q(p) dp. \tag{3.17}$$

In the actual calculation, the integrated value from the upper boundary

$$Q(p) = \int_0^p q(p) dp \tag{3.18}$$

is used instead of $q(p)$ to make the calculation faster. The values of Q at the half levels are obtained from

$$Q(p_{k+1/2}) = \int_0^{p_{k+1/2}} q(p) dp = \sum_{l=k+1}^{K} q_l \Delta p_l \tag{3.19}$$

There are several methods for calculating the distribution of $Q(p)$ from $Q(p_{k+1/2})$ and q_k. To calculate material transport, such as of water vapor, the Piecewise Rational Method (PRM; Xiao and Peng, 2004), a monotonic and conservative method, is used. For the advection of T and $\mathbf{v}_H$, the cubic Lagrange interpolation method is used. $Q(\tilde{p}_{k+1/2})$ is obtained from the $Q(p)$ distribution, and $\tilde{q}_k$ is calculated from

$$\tilde{q}_k = \frac{1}{\Delta \tilde{p}_k} \{Q(\tilde{p}_{k-1/2}) - Q(\tilde{p}_{k+1/2})\}, \tag{3.20}$$

which is derived from Eqs. (3.17) and (3.18).

This scheme for the vertical flux calculation is basically the same as that for the vertical coordinate transformation in the Scup coupler (Yoshimura and Yukimoto, 2008). The vertical flux calculation can also be considered a vertical coordinate transformation.

In step ③, the horizontal advection is calculated by a conventional semi-Lagrangian scheme. A quasi-cubic interpolation method (Ritchie et al., 1995) is used for horizontal interpolation. A quasi-fifth-order interpolation method is used only for the advection of horizontal wind, to improve precision. A correction method similar to that described by Priestley (1993) and by Gravel and Staniforth (1994) is used for global conservation in the calculation of material advection.

3.1.3. Time integration method

A generalized prognostic equation from Eqs. (3.1) through (3.4),

$$\frac{dX}{dt} = F(X),\tag{3.21}$$

is considered. A two-time-level semi-implicit semi-Lagrangian scheme (e.g., Temperton et al., 2001) and SETTLS (Hortal, 2002) are adopted to discretize Eq. (3.21) as

$$\frac{X^+ - X_D^0}{\Delta t} = \frac{1}{2}\left\{F^{(+)} + \beta\left(-L^0 + L^-\right)\right\}_D + \frac{1}{2}\left\{F^0 + \beta\left(-L^0 + L^+\right)\right\}\tag{3.22}$$

$$F^{(+)} \equiv 2F^0 - F^-,\tag{3.23}$$

where Δt is a time-step; $L(X)$ is the linearized term of $F(X)$; the subscript D means the three-dimensional departure point; the superscripts –, 0, and + mean past time $(t - \Delta t)$, present time (t), and future time $(t + \Delta t)$, respectively; and the superscript (+) means the future time by time extrapolation. β is a second-order decentering parameter and is set to 1.2, slightly larger than 1.0, which enhances the stabilizing effect of the semi-implicit scheme. Since the right-hand side of Eq. (3.22) is the time average of the present time and the future time and the spatial average of the departure point and the arrival point, Eq. (3.22) has second-order precision in time and space. Equation (3.22) is transformed as

$$X^+ - \frac{1}{2}\beta\Delta t L^+ = \left[X^0 + \frac{1}{2}\Delta t\left\{F^{(+)} + \beta\left(-L^0 + L^-\right)\right\}\right]_D + \frac{1}{2}\Delta t\left\{F^0 + \beta\left(-L^0\right)\right\}.\tag{3.24}$$

The right-hand side of Eq. (3.24) is calculated explicitly. The value at the three-dimensional departure

point is obtained by the advection calculation with the vertically conservative semi-Lagrangian scheme. Since L^+ is a linear function of X^+, X^+ can be obtained from Eq. (3.24). In spectral models, Eq. (3.24) can be solved independently of the horizontal wavenumber and therefore X^+ can be obtained easily.

3.2. Cumulus convection

3.2.1. Arakawa-Schubert-type scheme

The Arakawa-Schubert (AS)-type scheme (Arakawa and Schubert, 1974), one of the most popular for cumulus convection parameterization, is based on the assumption that there exists an ensemble (or group) of cumulus clouds at various heights in one grid column of the model, and that each individual cumulus cloud of the ensemble occupies a sufficiently small area of the grid. The updraft within the cumulus convection, by which heat and moisture are carried to the upper level while condensing the saturated moisture, and dry cold air from the surroundings is taken in (a process called entrainment), is parameterized by the cloud model. The generation of convection and its strength are determined by the destabilization of the grid-scale stratification, which is evaluated by the cloud work function (Arakawa and Schubert, 1974). The ensemble effect of the cumulus convection on the compensated subsidence and cloud top detrainment is parameterized by the cloud mass flux method. The JMA's operational scheme, though based on the original scheme of Arakawa and Schubert (1974), has been improved and developed variously.

Some of the modifications are the following:

1. A prognostic mass flux method is used to express the condition of away from quasi-equilibrium (Randall and Pan, 1993a, 1993b; Pan and Randall, 1993, 1998)

2. The cumulus downdraft is also considered (Cheng and Arakawa, 1997).

3. A mid-level convection scheme is included to express the mid-latitude convection accompanying the front and synoptic-scale disturbances.

Cumulus updraft

In an AS-type scheme, an ensemble of cumulus clouds at various heights is assumed, which the cloud base is at the top of the boundary layer. The prognostic equations for the cloud base mass flux are as follows:

$$A = \int_{Z_B}^{Z_T} g \frac{T^u - \overline{T}}{\overline{T}} \eta dz = \int_{Z_B}^{Z_T} g \frac{s^u - \overline{s}}{C_p \overline{T}} \eta dz \qquad (3.25)$$

$$\frac{\partial M_B^u}{\partial t} = F(A, M_B^u) \qquad (3.26)$$

Here A is the cloud work function; T^u and s^u are the temperature and the dry static energy, respectively, of a parcel in the cumulus updraft; T and s are the temperature and dry static energy, respectively, of the environment; M_B^u is the cloud base mass flux; and η is the standardized mass flux, which depends on the cloud base mass flux. F is the function of the damping formulation based on Randall and Pan (1993a, 1993b) and Pan and Randall (1998). Some modifications of function F are adopted in MRI-AGCM3. The top of each cumulus cloud corresponds to one vertical level in the model, and the ensemble size (i.e., the number of cumulus clouds) depends on the vertical resolution of the model.

In each cumulus cloud, an entrainment rate λ and a mass flux M^u is assumed:

$$\frac{1}{M^u} \frac{dM^u}{dz} = \lambda \qquad (3.27)$$

so,

$$M^u = M_B^u \exp(\lambda(z - z_B)) \qquad (3.28)$$

The suffix B refers to the cloud base level.

To reduce computational costs, Eq. (3.28) is linearized following Moorthi and Suarez (1992),

$$M^u = M_B^u (1 + \lambda(z - z_B)) = M_B^u \eta . \qquad (3.29)$$

Therefore, the sub-grid-scale values of each cumulus cloud, such as the mass flux and entrainment rate and the cloud work function, can be estimated from the grid-scale values of these parameters. The cloud base mass flux M_B is a role of the closure in the AS parameterization. In MRI-AGCM3, the cloud base is fixed and it is assumed that detrainment occurs only from the cloud top. Additionally, a minimum value of λ is set, and a cumulus cloud with $\lambda = 0$ is excluded (Tokioka et al., 1988).

Cumulus downdraft

In convective clouds, there are not only a vertical updraft but also a strong downdraft, caused by cooling due to evaporation of raindrops and the loading of precipitation particles. Heating and drying of the lower layer become excessive, compared with observation, if this downdraft is not considered (Arakawa and Cheng, 1993), so it is necessary to parameterize it. In MRI-AGCM3, a simplified method instead of that of Arakawa and Cheng (1993) is used. The cumulus downdraft is expressed not as a cloud ensemble like the cumulus updraft but as a single cumulus cloud. The downdraft is assumed to start from a height that is above the cloud base and where the cloud base mass flux of the updraft becomes half .

It is also assumed that entrainment and detrainment rates have the same values above the cloud base and only the detrainment rate is considered beneath the cloud base.

Mid-level convection

Convection due to frontal system and mid-latitude synoptic-scale disturbances is not expressible with an AS-type scheme because that scheme assumes that the cloud base is above the boundary layer or at a fixed low level. Therefore, cumulus convection must be expressed by the root of the convection in such a free atmosphere. This is called a mid-level convection scheme.

The conditions associated with mid-level cumulus convection are as follows:

1. There should exist above the cloud base level a higher moist static energy than the one determined by the AS scheme.

2. This level is the cloud base of the mid-level cumulus convection.

3. There should exist an upward motion of the grid scale.

Only one cumulus cloud is assumed, and an ensemble is not considered. A constant entrainment rate is given beforehand, allowing the cloud top level and the vertical profile of the mass flux to be estimated.

The closure assumption is based on the cloud work function, but the buoyancy effect is strengthened according to the strength of the upward motion.

3.2.2. Yoshimura cumulus scheme

A new mass-flux-type cumulus scheme has also been developed (Yoshimura et al. in preparation; hereafter, the Yoshimura cumulus scheme) that considers an ensemble of convective updrafts between the minimum and maximum turbulent entrainment/detrainment rates. Traditional mass-flux-type cumulus schemes can be divided largely into two types: the AS type and the Tiedtke (1989) type. In an AS-type scheme, multiple convective updrafts with different heights depending on entrainment rates are explicitly calculated, but each updraft is represented as a simple entraining plume for computational efficiency. In a Tiedtke-type scheme, only a single convective updraft with a certain turbulent entrainment/detrainment rate is calculated, but the updraft is represented as a more detailed entraining and detraining plume. In the Yoshimura cumulus scheme, convective updrafts with the minimum and maximum entrainment/detrainment rates are calculated as detailed entraining and detraining plumes as in a Tiedtke-type scheme, and multiple convective updrafts with different heights as in an AS-type scheme are represented by considering continuous convective updrafts between the minimum and maximum turbulent entrainment/detrainment rates.

Convective updraft

In the Yoshimura cumulus scheme, organized entrainment, organized detrainment, turbulent entrainment, and turbulent detrainment are considered in the convective updraft (Fig. 4), as in the Tiedtke cumulus scheme.
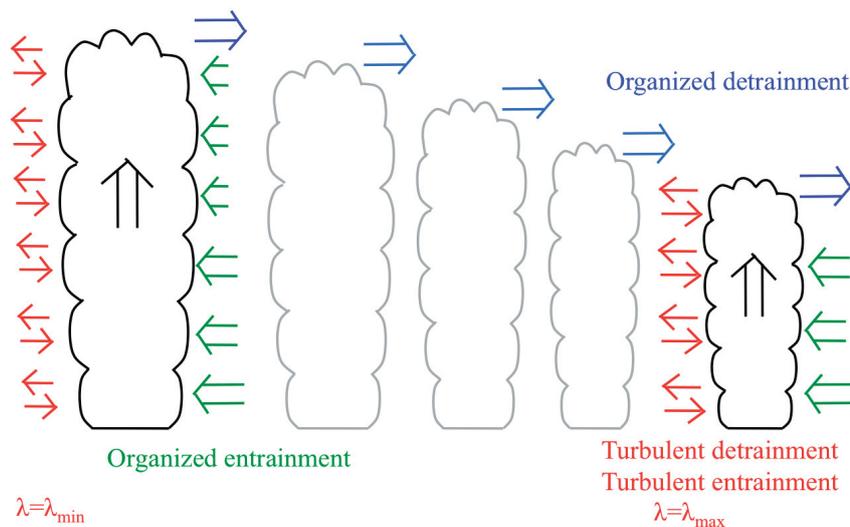

Figure 4 Schematic diagram for convective updraft. Red arrows indicate turbulent entrainment/detrainment. Green and blue arrows indicate organized entrainment and organized detrainment respectively. The left end (right end) is convective updraft with minimum entrainment rate λ_{min} (maximum entrainment rate λ_{max}). Convective updrafts between minimum and maximum entrainment rates are continuously present.

Two kinds of organized entrainment are considered. One is entrainment from a layer with large moist static energy from which updrafts originate. When the air with large moist static energy is in the boundary layer, the usual (deep or shallow) convection occurs. When it is above the boundary layer, mid-level convection occurs. The second kind is entrainment nearly proportional to the grid-scale mass convergence and the convective updraft mass flux.

Turbulent entrainment and detrainment are proportional to the convective updraft mass flux. The turbulent entrainment and detrainment rates are set to the same value. The minimum turbulent entrainment/detrainment rate λ_{min} is set to 0.5×10^{-4} m^{-1}, and the maximum λ_{max}, at the cloud bottom, is set to 3.0×10^{-4} m^{-1}. Two convective updrafts, one with the minimum and one with the maximum turbulent entrainment/detrainment rates, are calculated. Convective updrafts between the minimum and maximum entrainment rates are assumed to be continuously present. Temperatures, virtual temperatures, water vapor mixing ratios, turbulent entrainment/detrainment rates, and other variables in the convective updrafts are obtained by linear interpolation between the two convective updrafts with the minimum and the maximum entrainment rates. When the virtual temperature of a convective updraft is lower than the virtual temperature in the environment at some vertical level, the convective updraft becomes negatively buoyant, leading to organized detrainment at that level.

In the Yoshimura cumulus scheme, the number of calculations is $O(N)$, where N is the number of vertical model levels. In an AS-type cumulus scheme, the number is $O(N^2)$ if each convective updraft is calculated as a detailed entraining and detraining plume. The Yoshimura cumulus scheme is superior in this respect.

Closure assumption

Magnitudes of the convective updrafts are determined by using a closure assumption (Nordeng, 1994), which is based on convective available potential energy (CAPE). First, the convective updrafts are provisionally calculated by assuming that convective updrafts are uniformly present between the minimum and maximum entrainment rates. The provisional mass flux of Cumulus k is obtained, where Cumulus k is defined as the cumulus cloud that contains the convective updrafts whose cloud top is at the k-th vertical level. Next, the magnitude of the mass flux of Cumulus k is estimated by assuming that Cumulus k reduces CAPE$(k) \times a(k)$ in a relaxation time τ, where CAPE(k) is the CAPE of Cumulus k and $a(k)$ is the proportion of the provisional mass flux of Cumulus k at the cloud bottom.

The sum of $a(k)$ is 1.0.

Convective downdraft

A part of the sum of the detrainments from the convective updrafts is equally mixed with the environment air, which is saturated and cooled to the wet-bulb temperature by evaporation of cloud water and precipitation at each vertical level. When the mixture is negatively buoyant, it originates a convective downdraft. A single convective downdraft is calculated. The negatively buoyant mixture becomes the organized entrainment to the convective downdraft. The turbulent entrainment/detrainment rate is 2.0×10^{-4} m^{-1}. The mass flux of the convective downdraft is limited to not more than 0.3 times the sum of the mass fluxes of the convective updrafts. When the convective downdraft becomes positively buoyant at some level, the entire downdraft mass flux is detrained at that level as organized detrainment. If the downdraft does not become positively buoyant, organized detrainment from the downdraft occurs at the sub-cloud layer.

Vertical transport

In the Yoshimura cumulus scheme, a conservative and monotonic semi-Lagrangian scheme is used for vertical transport by convection. The PRM is used for vertical interpolation of prognostic variables in the environment. This is the same method as that used for vertical flux calculation in the dynamics process described in Section 3.1.2. This semi-Lagrangian scheme relaxes the time-step limitation imposed by the CFL condition and enables positive-definite natural material transport.

Horizontal momentum transport

The vertical transport of horizontal momentum by convection is calculated. It is overestimated unless the effect of the sub-grid-scale horizontal pressure gradient force, which acts to adjust the direction of the horizontal wind in convection toward that of the wind in the environment, is introduced. A scheme based on that of Gregory et al. (1997) is adopted for the pressure gradient force. In this scheme, the pressure gradient force is set proportional to the vertical wind shear in the environment.

3.2.3. Kain-Fritsch scheme

The Kain-Fritsch (KF) scheme was developed for application to a meso-scale convection system (Kain and Fritsch, 1990, 1993; Kain, 2004). It assumes a one-dimensional cloud model in which cumulus updraft, entrainment of the surrounding cold, dry air, and detrainment from the updraft, are estimated at each vertical level. Entrainment and detrainment are considered not only at the cloud top and base but also at the sides of the cloud. A trigger function based on CAPE is used to generate convection. Convection removes the vertical instability of the grid scale while consuming CAPE. This scheme has been applied in JMA's operational regional model (Saito et al., 2001, 2006, 2007).

Cumulus updraft

One characteristic feature of a KF scheme is the method for determining entrainment and detrainment of the parameterized cumulus convection, in which entrainment and detrainment are considered not only at the cloud base and cloud top but also at each vertical level between them. It is assumed that there always exist many minute parts caused by mixing of the cloud updraft air with the surrounding air in various proportions, and that minute parts that acquire negative buoyancy drop out of the updraft (detrainment) whereas those with positive buoyancy flow into the cloud updraft (entrainment). Therefore, it is necessary to estimate the degree to which the cloud updraft mixes with the surrounding air. This mixing ratio is determined from the vertical atmospheric pressure, the upward mass flux of the cloud base, and the radius of the updraft. Refer to Kain and Fritsch (1990) and Kain (2004) for details. When the mixing ratio is small, the surrounding dry, cold air flow into the updraft (entrainment) is reduced and outflow of the moist, warm updraft air into the surrounding air is decreased, so the cloud top becomes higher. The cloud top is assumed to be at the level at which the temperature of the updraft parcel is equal to that of the surrounding air. In other words, the cloud top can be considered to intrude into the stable stratification (called overshooting).

Closure assumption

The closure assumption of the KF scheme adopts a method for removing the grid-scale CAPE by parameterized cumulus convection and adjusting the mass flux following Bechtold et al. (2001). The removal ratio can be set as a parameter.

Cumulus downdraft

In the KF scheme, the downdraft is caused by cooling by evaporation of the condensation. The downdraft starts at a saturated level that is more that 150 hPa above the lifting condensation level (LCL). Further, entrainment occurs only above the LCL; under the LCL, humidity decreases with height; and detrainment occurs only under the LCL. The downdraft method is simplified compared with that used for determining the entrainment and detrainment of the updraft.

Trigger function

A trigger function is used in the KF scheme to judge whether sub-grid-scale convection is generated. The trigger function is composed three terms: the temperature of the LCL (T_{LCL}), the temperature perturbation that depends on the buoyancy at the LCL (ΔT_{LCL}) (Kain, 2004), and the temperature perturbation that depends on the humidity (ΔT_{RH}) (Undén et al., 2002). When the trigger function ($T_{LCL} + \Delta T_{LCL} + \Delta T_{RH}$) has a value higher than the surrounding temperature, parameterized cumulus convection is generated.

Conversion of condensation to precipitation

In MRI-AGCM3, two different schemes can be used to generate precipitation with the KF scheme, one by Ogura and Cho (1973) and the other by Kessler (1969). Both schemes estimate the proportion of detrained condensed water from the updraft that falls as precipitation. We adopt the latter method in MRI-AGCM3 when the KF scheme is used for cumulus parameterization.

3.3. Radiation

The radiation processes in MRI-AGCM3 are briefly described here. For the most part, the radiation scheme is the same as that of JMA's operational global atmospheric model (see details in Numerical Prediction Division/JMA, 2007), but there are some differences, for example, in the interaction with aerosols. Because of relatively large computational costs, radiation processes are often calculated at coarser spatial and temporal scales than otherwise used in a model. In the standard ESM configuration, the full radiation computations are calculated for every two grids in the zonal direction, and for every hour and every 3 hours in the shortwave and longwave regions, respectively.

3.3.1. Radiative transfer model

In MRI-AGCM3 radiation scheme, infrared (i.e., longwave, hereafter LW) radiation of up to 3000 cm^{-1} and solar (shortwave, hereafter SW) radiation are treated separately. The LW region of the spectrum is divided into 9 bands (see Figure 5), and the SW region into 22 bands (see Figure 6). The radiative flux is calculated in each band. The model column is split into plane-parallel, homogeneous layers and vertical radiative transfer is solved numerically. In the LW scheme, the absorption approximation method is adopted and band-integrated upward and downward radiative fluxes are calculated by using the band-emissivity method with a diffusivity factor. In the SW scheme, a two-stream approximation (δ-eddington approximation; Joseph et al., 1976) method is used to solve direct and diffuse flux at each layer boundary. Downward (upward) diffuse fluxes in a column are calculated in descending (ascending) order, from the top to the bottom (the bottom to the top) level (as in APPENDIX A in Briegleb, 1992).

Figure 5   Spectral bands and absorber gases for LW. Letter T and K mean line absorptions calculated by table lookup method and k-distribution method, respectively. Letter C means use of parameterization for water vapor continuum absorption.

Figure 6   Spectral bands and absorber gases for SW. ESF means use of exponential sum fitting technique and F&R means employment of parameterization based on Freidenreich and Ramaswamy (1999).

3.3.2. Atmospheric radiation

In the LW and SW schemes, major absorptions due to water vapor (line and continuum absorption), carbon dioxide (e.g., in the 15 μm band and near-infrared region), and ozone (in the 9.6 μm band and the visible and ultraviolet regions) are considered. In addition, absorptions due to

methane (CH_4), dinitrogen monoxide (N_2O), and CFCs are taken into account in the LW scheme for their greenhouse effect. Absorption by oxygen and Rayleigh scattering by molecules of atmospheric gas are also calculated in the SW scheme.

In the LW scheme, absorption due to atmospheric gas is evaluated by the Planck weighted transmission function in each spectral band. Two types of parameterization obtained from an offline line-by-line (LBL) calculation based on a database of absorption lines are used in order to calculate line absorptions. If the effect of Doppler line broadening cannot be ignored in the stratosphere, a transmittance table made by LBL pre-computations for some pressures, temperatures, and absorber concentrations is referred (Chou and Kouvaris, 1991). This table was calculated by using the HITRAN 2000 (update 1; Rothman et al., 2003) line database and the LBLRTM (Clough et al., 1992) calculation package. For the other absorptions in which the Lorentz type of line broadening is just dominant, the transmittance is rapidly calculated by the k-distribution method (Arking and Grossman, 1972) with the absorber amount scaled by atmospheric pressure and temperature. For the continuum absorption of water vapor, self- and foreign-broadened absorption are considered after the method of Zhong and Haigh (1995) but updated with absorber coefficients from MT-CKD version 1.0, a refined version of the CKD continuum model (Clough et al., 1989).

The SW scheme calculates the optical depth of each absorption due to atmospheric gases. Absorption due to water vapor is calculated by the 7-band k-distribution method (or the exponential sum fitting technique; Lacis and Hansen, 1974) after Briegleb (1992). For ozone, carbon dioxide, and oxygen, the parameterization of Freidenreich and Ramaswamy (1999) is used to compute optical depth of the absorption. Their work is also referred in determining the Rayleigh scattering coefficients.

3.3.3. Cloud radiation and aerosol effect

To represent the direct effects of aerosols, optical parameters are configured for 5 aerosol species corresponding to those in the aerosol model (Section 6): sulfate, black carbon (soot), organic carbon, mineral dust, and sea-salt. The extinction and absorption coefficients and asymmetry factors of these species are computed under the assumption of Mie scattering by spherical particles by using the complex refraction index data of OPAC software (Hess et al., 1998). In the case of hygroscopic species, their dependence on ambient relative humidity is also considered (Chin et al., 2002).

The effect of aerosols on the optical properties of clouds (i.e., the first indirect effect) is considered in the configuration of the effective radius of cloud particles. The effective radius of a liquid water cloud particle is computed as a function of cloud droplet number density, based on Liu et al. (2006) and Peng and Lohmann (2003). If a two-moment scheme is selected for the cloud scheme (Section 3.4), then the aerosol indirect effect on ice cloud particles is also considered (Lohmann, 2002). Otherwise, the effective radius of ice cloud particles is parameterized as a function of temperature and ice-water content (Wyser, 1998).

In terms of the optical properties of cloud particle, LW emissivity is parameterized depending on cloud water content (Kiehl and Zender, 1995), and the corresponding absorption coefficient is parameterized as a function of effective radius (Hu and Stamnes, 1993, for liquid water clouds, and Ebert and Curry, 1992, for ice clouds). Optical depth, single scattering albedo, and the asymmetry factor in SW are similarly parameterized by cloud water content and effective radius (Slingo, 1989, for water clouds and Ebert and Curry, 1992, for ice clouds).

Though a cloud is approximated as a black body in the LW scheme, the calculation method of Räisänen (1998) is adopted, in which both cloudiness and cloud emissivity in a cloudy layer are properly considered and the calculation results have no dependency on the vertical resolution of the model layers. The vertical overlap of clouds greatly influences estimations of radiative fluxes in a cloudy column. In the LW scheme, maximum-random overlap (Geleyn and Hollingsworth, 1979) is assumed. In the SW scheme, total cloudiness in a column is first computed according to the maximum-random overlap assumption, and then random overlap is assumed to solve radiative fluxes in a cloudy sub-column.

3.4. Cloud model

Cloud water and fraction are the variables of the cloud scheme used to represent large-scale condensation in the AGCM. The Smith cloud scheme (Smith, 1990), which is based on probability distributions (Sommeria and Deardorff, 1977), is employed in JMA's operational weather prediction model. The Tiedtke cloud scheme (Tiedtke, 1993; ECMWF, 2004; Jakob, 2000), which treats cloud water and fraction as prognostic variables, is also incorporated in MRI-AGCM3.

In MRI-ESM1, the chemistry climate model (MRI-CCM2) and the aerosol model (MASINGAR mk-

2) can be coupled via the Scup coupler with MRI-AGCM3. This means that MRI-AGCM3 is able to recognize the spatial-temporal distribution of aerosol species. For projection of future global climate change, direct and indirect effects of aerosols are the primary factors leading to uncertainties in the assessment of radiative forcing, and they are therefore among the most important physical processes coupling the aerosol model with the AGCM. To represent the indirect effects of aerosols in detail, cloud droplet and ice crystal concentrations are important information. Furthermore, their efficient simulation is desirable for long-term predictions of the ESM. To increase the accuracy of the indirect aerosol effects in the ESM, it is necessary for the cloud scheme, which is represented by the cloud water mixing ratio and fraction, to be expanded to take into consideration at least the cloud liquid water mixing ratio, the cloud ice mixing ratio, cloud droplet and ice crystal concentrations, and cloud fraction.

Therefore, a new two-moment bulk cloud scheme (called the MRI-TMBC scheme) was developed by expanding the original equation system (i.e., prediction of the cloud water mixing ratio by the Tiedtke cloud scheme) to include the necessary variables. The new scheme predicts the cloud liquid water mixing ratio, the cloud ice mixing ratio, and cloud droplet and ice crystal concentrations (shown schematically in Fig. 7). The Smith, Tiedtke, and MRI-TMBC schemes can be arbitrarily selected in MRI-ESM1. The MRI-TMBC scheme is described by differential equations as follows.

$$\frac{\partial q_c}{\partial t} = adv(q_c) + S_{conv}^{liq} + S_{new}^{liq} + S_{old}^{liq} - E^{liq} - G^{rain} - (N_{imm} + N_{cont} + N_{homo}) + M_{melt} \tag{3.30}$$

$$\frac{\partial q_i}{\partial t} = adv(q_i) + S_{conv}^{ice} + S_{new}^{ice} + S_{old}^{ice} - E^{ice} - G^{snow} + (N_{imm} + N_{cont} + N_{homo}) - M_{melt} \tag{3.31}$$

$$\frac{\partial q_v}{\partial t} = adv(q_v) - (S_{conv}^{liq} + S_{new}^{liq} + S_{old}^{liq} + S_{conv}^{ice} + S_{new}^{ice} + S_{old}^{ice}) + E^{liq} + E^{ice} + E^{rain} + E^{snow} \tag{3.32}$$

$$\frac{\partial N_c}{\partial t} = adv(N_c) + NS_{conv}^{liq} + NS_{new}^{liq} - NE^{liq} - NG^{rain} - (NN_{imm} + NN_{cont} + NN_{homo}) + NM_{melt} \tag{3.33}$$

$$\frac{\partial N_i}{\partial t} = adv(N_i) + NS_{conv}^{ice} + NS_{new}^{ice} - NE^{ice} - NG^{snow} - (NN_{imm} + NN_{cont} + NN_{homo}) - NM_{melt} \tag{3.34}$$

where q_c, q_i, and q_v respectively indicate the cloud liquid water mixing ratio, the cloud ice mixing ratio, and the water vapor mixing ratio (kg kg^{-1}); N_c and N_i are respectively the cloud droplet concentration and the ice crystal concentration (m^{-3}); and S, E, G, N, M, and adv respectively represent the source, evaporation, precipitation, the interaction between cloud water and cloud ice, melting, and advection

terms. In addition, the superscripts *liq*, *ice*, *rain*, and *snow* respectively represent the cloud liquid water, cloud ice, rainfall, and snowfall components, and the subscripts *conv*, *new*, and *old* respectively represent the convective, stratiform formation, and stratiform growth components. Finally, the subscripts *imm*, *cont*, and *homo* represent immersion freezing, contact freezing, and homogeneous freezing, respectively. The differential equations for cloud droplet concentration and ice crystal concentration are formally described to be consistent with those for the cloud liquid water mixing ratio
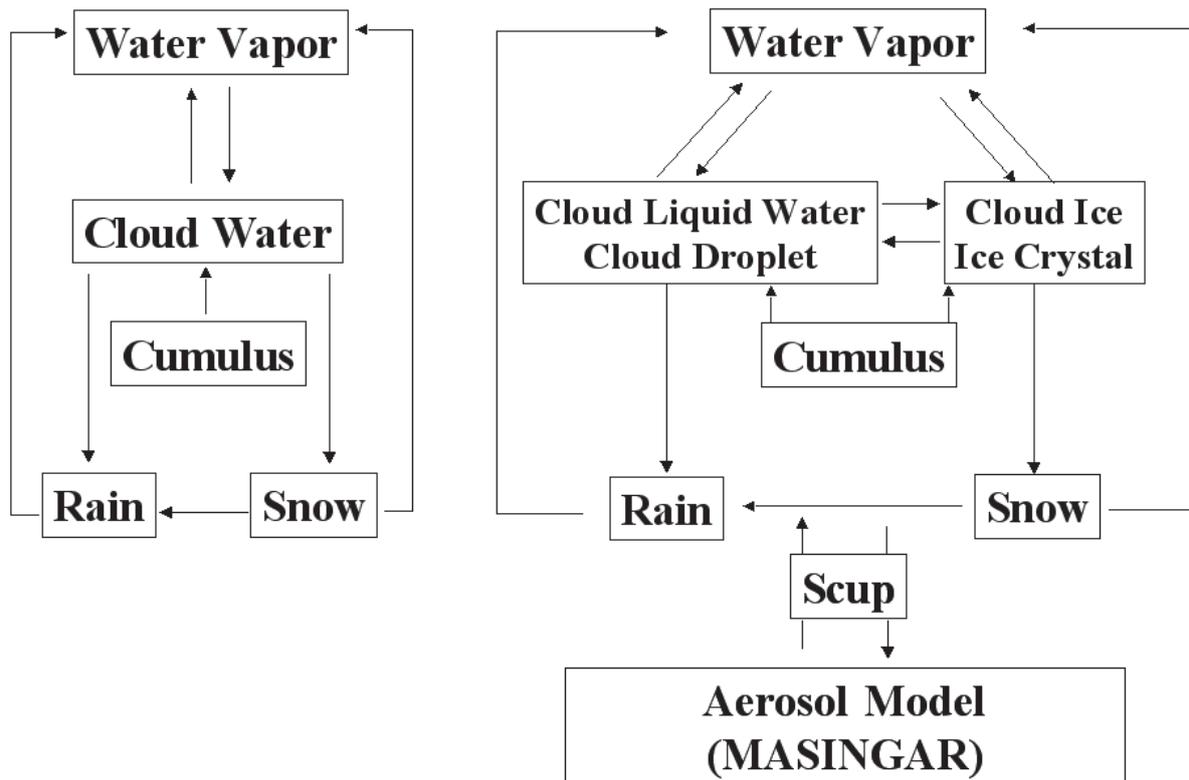

Figure 7   Framework of cloud scheme in the MRI-ESM1. Left figure indicates framework of the Smith cloud scheme and the Tiedtke cloud scheme. Right figure indicates a newly modeled double moment bulk cloud scheme.

and cloud ice mixing ratio.

The aerosol model is directly coupled to the MRI-TMBC scheme by activation of aerosol species into cloud droplets and ice crystals. The aerosol species employed in both MASINGAR mk-2 and the cloud scheme are SO_x + dimethyl sulfide (DMS), black carbon (BC), organic carbon (OC), sea salt (2 bins), and dust (6 bins). The activation of some aerosols into cloud droplets is based on the parameterizations of Abdul-Razzak and Ghan (2000, 2002) and Takemura et al. (2005). The activation of some aerosols into ice crystals is based on the parameterizations of Bigg (1953, immersion freezing), Lohman and Diehl (2006, contact freezing), and Kärcher et al. (2006, cirrus clouds). Cloud droplet and

through their effective radii.

The deposition and depositional growth terms are based on Murakami (1990) and Rutledge and Hobbs (1983), respectively, and the condensation and condensation growth terms on Tiedtke (1993). Melting occurs when the atmospheric temperature is above 273.15 K, and homogeneous freezing occurs at temperatures below 235.0 K. A semi-Lagrangian scheme (Section 3.1) is used for the advection process. The precipitation process is basically unchanged, except that the parameterization of Rotstayn (2000) is adopted for the rainfall term (Fig. 7). The Bergeron-Findeisen process is also incorporated into the MRI-TMBC scheme. This process occurs when the cloud ice mixing ratio is greater than 0.5 mg kg^{-1} (Lohman et al., 2007). Furthermore, a saturation adjustment proposed by Tao (1989) is introduced

3.5. Planetary boundary layer

The role of the boundary layer scheme in AGCM is to parameterize the vertical transport of momentum, heat, and moisture by turbulence in the atmosphere. The boundary layer scheme in JMA's operational model is the turbulence model advocated by Mellor and Yamada (1974, 1982) (the MY scheme), which is a second-order closure model based on the Reynolds averaging method. However, in the new MRI-AGCM3, the evaluation of the closure constants and the mixing length are optionally modified, following Nakanishi (2001) and Nakanishi and Niino (2004, 2006, 2009).

Additionally, a non-local scheme based on the parameterizations of Troen and Mahrt (1986) and Holtslag and Boville (1993), which can express non-local vertical mixing when conditions near the surface layer are unstable, is an optional PBL scheme that can be selected in MRI-AGCM3.

3.5.1. Mellor-Yamada scheme

The Mellor-Yamada scheme expresses the third moment quantity by the second moment by using the Reynolds averaging method. In all, there are 15 prognostic variables of the second moment (the Level 4 model), but in weather and climate models the scheme can be simplified according to the contribution of anisotropy because of the computational costs (Levels 3, 2.5, and 2; see Mellor and Yamada, 1974, 1982, for details). In Level 2, used in MRI-AGCM3, all prognostic equations become diagnostic ones, and all variables of the second moment are obtained by solving those equations. In addition, in the atmospheric boundary layer, because the horizontal variation of physical values is very

small compared with the vertical variation, horizontal differentiation is disregarded. This approximation is called the boundary layer approximation. In general, there exist two or more closure constants in the closure model. These constants should be determined empirically. Mellor and Yamada (1982) determined these closure constants from observations and wind tunnel experiments under neutral conditions. Moreover, the mixing length l is given beforehand:

$$\frac{1}{l} = \frac{1}{L_S} + \frac{1}{L_T} \tag{3.35}$$

$$L_S = \kappa z \tag{3.35a}$$

$$L_T = \alpha \frac{\int_0^\infty qz\,dz}{\int_0^\infty q\,dz} \tag{3.35b}$$

where L_S is the length determined according to the vertical log-profile of the physical value near the surface, L_T is the length reflecting the vertical profile of turbulent energy (q), α is an empirical constant, and κ is the Karman constant.

3.5.2. Mellor-Yamada-Nakanishi-Niino scheme

Nakanishi (2001) and Nakanishi and Niino (2004, 2006, 2009) proposed an improved version of the MY scheme (called the MYNN scheme) for determining closure constants, mixing length, and the stability of time integration. We introduced the first two improvements into MRI-AGCM3 as follows. First, on the basis of data obtained by large eddy simulation (LES), the MYNN scheme re-evaluates the closure constants and introduces terms for the effect of buoyancy and wind shear, which are neglected in MY model.

$$(A_1, A_2, B_1, B_2, C_1) = (0.92, 0.74, 16.6, 10.1, 0.08) \rightarrow (1.18, 0.665, 24.0, 15.0, 0.137) \tag{3.36}$$

$$(C_2, C_3, C_4, C_5) = (0,\ 0,\ 0,\ 0) \rightarrow (0.65, 0.294, 0, 0.2) \tag{3.37}$$

Here, C_2 and C_3 reflect the effect of buoyancy, and C_5 that of wind shear. Refer to the original paper for details.

Second, a new diagnostic equation for the mixing length l, which was considered an uncertain expression, is proposed here, based on LES:

$$\frac{1}{l} = \frac{1}{L_S} + \frac{1}{L_T} + \frac{1}{L_B} \tag{3.38}$$

$$L_S = \begin{cases} \kappa z / 3.7 & (\zeta \geq 1) \\ \kappa z /(1 + 2.7\zeta) & (0 \leq \zeta < 1) \\ \kappa z (1 - \alpha_4 \zeta)^{0.2} & (\zeta < 0) \end{cases} \tag{3.38a}$$

$$L_T = \alpha_1 \frac{\int_0^\infty qz\,dz}{\int_0^\infty q\,dz} \tag{3.38b}$$

$$L_B = \begin{cases} \alpha_2 q / N_1 & (\partial\theta/\partial z > 0, \zeta \geq 0) \\ [\alpha_2 q + \alpha_3 (q_c / L_T N_1)^{1/2}]N_1 & (\partial\theta/\partial z > 0, \zeta < 0) \\ \infty & (\partial\theta/\partial z \geq 0) \end{cases} \tag{3.38c}$$

where α_1, α_2, α_3, and α_4 are empirical constants (= 0.23, 1.0, 5.0, and 100.0, respectively); $\zeta = z/L$; and L is the Monin-Obukhov length. This new equation thus evaluates the stability of the surface layer by using the Monin-Obukhov length and the effect of buoyancy (L_B) (Hara, 2007ab).

3.5.3. Non-local scheme

When conditions near the surface are unstable, especially in the daytime, momentum, heat, and moisture are often very efficiently transported through the entire boundary layer by the large turbulence in the PBL. Such characteristic large turbulence transport is called the non-local effect. We introduced a scheme to express these non-local effects following Troen and Mahrt (1986) and Holtslag and Boville (1993). However, it is well known that although this scheme can express well the development of a convective mixing layer in the daytime, it cannot adequately express the weakening of the mixing layer and the influence of the diurnal cycle on surface temperature and wind. Moreover, in some cases, the cold pool is destroyed when a cold layer is formed in the boundary layer. Therefore, development of this scheme has been postponed for the present.

3.6. Land surface models

Three land-surface models are available in MRI-AGCM3, and a model user can select any one of them. The first one is JMA/SiB (Simple Biosphere model; Sellers et al., 1986, Sato et al., 1989), which is

used mainly for short-range weather forecasting. The second, SiB0109 (Hirai et al., 2007), which was developed for climate research purposes and is used in MRI-CGCM2.3, both water mass and energy are perfectly conserved. The third one, HAL (Hosaka et al., in preparation), is newly developed and will be used for the CMIP5 simulations. In this subsection, HAL is briefly described.

HAL (the name is formed from the first letters of Hydrology, Atmosphere, and Landsurface, and means "spring" in Japanese) is MRI-AGCM3's new land-surface model. The major predicted variables are temperature and moisture content in the vegetation, soil, and snow submodels, and HAL diagnoses surface conditions. HAL also evaluates heat, moisture, and momentum fluxes and albedo, which are used in MRI-AGCM3 simulations as lower atmospheric boundary conditions. HAL can calculate variables related to the terrestrial carbon cycle, and they are used by the terrestrial carbon model (Section 8.1).

HAL consists of three submodels: SiByl, SNOWA, and SOILA, which are coupled to one another by the LCUP land-surface coupler, which also connects HAL to MRI-AGCM3. LCUP supports the mosaic and mixture strategy (Koster and Suarez, 1996), which enables more appropriate fluxes to be estimated over non-uniform surfaces.

SiByl has surface vegetation processes similar to JMA/SiB, on which it is based. SiByl has 2 vegetation layers (canopy and grass) and calculates heat, moisture, and momentum fluxes between the land surface and the atmosphere. The major predicted variables are the temperature of the canopy and the surface skin, and the moisture content of the canopy and the grass. Included moisture processes are precipitation intercepted by and dropped from the canopy and the grass, evaporation or sublimation from and dew or frost on bare soil and vegetation, and transpiration by vegetation. Heat processes implemented comprise shortwave radiation (direct/diffuse, visible/infrared), longwave radiation, sensible heat, latent heat, and ground heat fluxes. A bulk formulation scheme (Louis, 1979) is used for estimating surface flux. Air surface information such as the air temperature at 2 m height is diagnosed.

Some physical processes are improved in HAL from JMA/SiB. The overly simplified snow and soil processes in JMA/SiB are not used in HAL. The ground heat flux is calculated not by the force restore method but by solving heat conduction equations with temperatures of the lower (snow or soil) layers. When the snow water equivalent (SWE) is less than ~20 mm, partial snow is realized. For the estimation of stomatal resistance, in addition to the original JMA/SiB method, a new option for biochemical photosynthesis process is available that is able to output some variables for the terrestrial

carbon model (Section 8.1) and to evaluate the CO_2 flux between the land surface and the atmosphere. In JMA/SiB, many vegetation parameters depend only on 13 vegetation types. In contrast, in HAL, the default values, which depend on the types, are replaced by more appropriate values based on observational data at each grid point.

The snow submodel SNOWA can have more snow layers[1] than SiB0109. The number of layers depends on the SWE and the snow accumulation history. The top layer is typically 10 mm SWE in thickness, and the thicknesses of the 2nd to 7th layers are 20 mm SWE. The lowest (8th) layer receives discharge from all the layers above it. Each layer also has an upper and lower SWE limit value. If the SWE of a snow layer exceeds the upper limit, the layer is divided into 2, and if it falls below the lower limit, the snow layer is combined with the layer beneath it. Therefore the snow properties are not affected by numerical diffusion so much.

The predicted variables for snow are temperature, SWE, density, and the aerosol contents[2] of each layer. To predict the temperature, heat conduction equations are solved where the upper boundary condition is the ground heat flux calculated by the upper submodel (SiByl). When the temperature of each layer is higher than -1 °C, a water phase change occurs. If the mixing ratio of liquid water is more than 10%, the excess liquid water drops into the layer below. If the temperature of the uppermost underlying soil layer is higher than 1 °C, the excess energy is used for melting the snow at the bottom of the layer, and the meltwater infiltrates into the soil. SNOWA also has some snow albedo schemes (options). The default setting uses the aerosol mixing ratio (Aoki et al., 2003), and in another option the albedo is predicted and changes depending on the temperature (Aoki and Tanaka, 2008).

The soil submodel SOILA is composed of 14 soil layers with depths of 2, 3, 5, 10, 10, 20, 30, 30, 40, 100, 100, 150, 200, and 300 cm, for a total depth of 10 m[3]. There are 5 layers in the top 30 cm, which allows diurnal temperature changes to be simulated. The temperature of each layer is predicted by solving heat conduction equations, where the upper boundary condition (heat flux) is given by an upper submodel (SiByl or SNOWA). The number of layers in which soil moisture is predicted depends on the vegetation type. For example, in forest grids, soil moisture is present in the uppermost 11 layers (the upper 350 cm), in grass grids in the uppermost 9 layers (150 cm), and in desert grids in the uppermost 6 layers (50 cm). The infiltration flux of liquid water is estimated by solving the Darcy

---

[1] The maximum number of snow layers and the typical upper and lower limits of SWE in each layer can be arbitrarily set by a user. The values described above are model defaults.

[2] Depending on the snow albedo schemes selected, the aerosol contents can be replaced with other parameters.

[3] The number of soil layers and their depths can be arbitrarily set by a user, with some limitations.. The values described above are model defaults.

equation, in which hydraulic conductivity depends on the soil moisture. Drainage (gravitational runoff) occurs from the bottom layer, and surface runoff occurs from the top layer. The phase change of water occurs between −1 °C and 1 °C, and in colder regions the soil is frozen.

3.7. Ocean surface processes

In this section, the modeling of sea-surface and sea-ice surface processes is described. An important function of the ocean surface scheme is the calculation of turbulent heat, moisture, and momentum fluxes. The atmospheric variables, the (skin) surface temperature, and the fluxes are determined at the same time by the implicit method from the vertical diffusivity, which is calculated in the PBL scheme. The fluxes are calculated by the generally used bulk method. The bulk coefficients are from Louis (1979) and Louis et al. (1982), except those for turbulent fluxes in the unstable state, which are from Miller et al. (1992).

3.7.1. Sea surface

Sea-surface temperature (SST) is fixed during each time step in the calculation of the fluxes over the sea surface. When the conventional sea-surface scheme is used, SST is read from a boundary conditions file (bulk SST) in a typical AGCM experiment. It is set to the same temperature as that in the first layer (typically a few meters thick) of the OGCM in a typical CGCM simulation. However, when the simple skin SST scheme described here is used, the skin temperature provided by the scheme is used in the AGCM as the lower boundary over the sea surface .

Simple skin SST scheme

This scheme is designed to represent short-term temperature variation (e.g., diurnal variation) at the air–sea interface caused by short-term variations in wind and solar radiation (Fig. 8). The interface temperature is estimated from the heat fluxes to the atmosphere and from the bottom of the layer. Since the sub-skin layer is empirically known to be apt to mix with the underlying layer under windy conditions, the coefficient for the heat flux from the bottom of the layer depends on wind speed, being larger when the wind is stronger (Kawai and Wada, 2007).

This scheme has one sub-skin layer with a linear temperature profile within the layer, and its thickness (h_s) is 1 m. The temperature at $h_s/2$ depth is the sub-skin SST (T_s), which is the prognostic
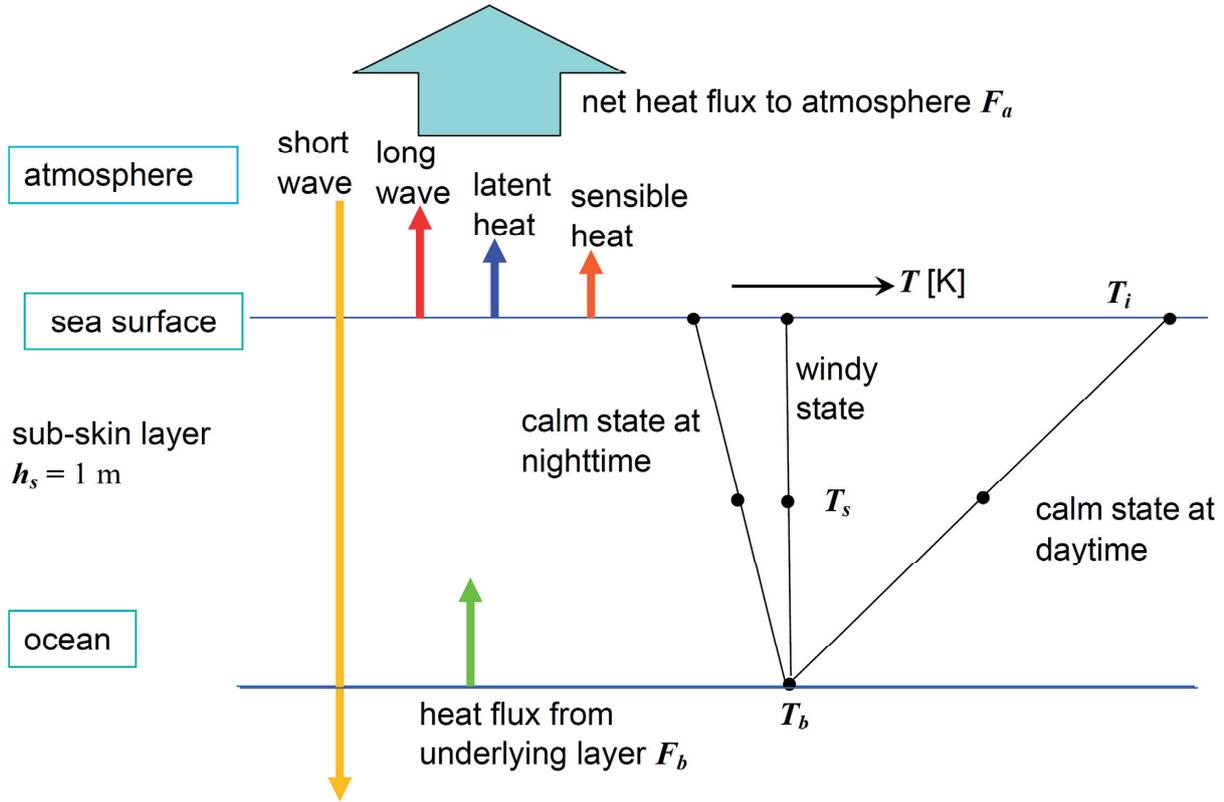
Figure 8   Conceptual illustration of the simple skin SST scheme

variable in the force restore method. The temperature at the bottom of the layer (T_b) is set as 'bulk SST' in this scheme. In AGCM, the bulk SST, T_b, is read from the boundary condition file, and in CGCM it is the first-layer temperature of the OGCM. The temperature at the top of the layer (T_i) is the interface SST, and is used for calculation of the fluxes at the next step. For simplicity, it is assumed that the temperature profile in the layer is linear:

$$T_i = T_b + 2(T_s - T_b) = 2\, T_s - T_b. \tag{3.39}$$

The tendency of the sub-skin SST is estimated by the following equation.

$$\rho\, C_p\, h_s\, dT_s\, /dt = F_b - F_a, \tag{3.40}$$

where ρ is the density of seawater (1030 kg m^{-3}), C_p is the specific heat of seawater (3930 J K^{-1} kg^{-1}), F_b is heat flux from bottom of the layer, and F_a is net heat flux to the atmosphere. Fluxes already calculated in this step are used for F_a, which includes latent heat, sensible heat, longwave radiation, and shortwave radiation flux. The shortwave radiation fluxes are calculated for visible and near-infrared wavelengths, taking penetration into account, with the following equation:

$$R_{sw} = R_{swvis}(1 - exp(-h_s/h_{pvis})) + R_{swnir}(1 - exp(-h_s\,/h_{pnir})), \tag{3.41}$$

where R_{sw} is solar radiation absorption in the sub-skin layer, R_{swvis} is net visible radiation at the surface (downward is positive), h_{pvis} is the *e*-folding depth for visible radiation (23 m), R_{swnir} is net near-infrared

radiation at the surface (downward is positive), and h_{pnir} is the e-folding depth for near-infrared radiation (0.35 m). F_b is estimated by the bulk equation,

$$F_b = \rho\ C_p\ h_s\ (T_b - T_s)\ /\ \tau. \tag{3.42}$$

(Notice that this equation uses T_s that would be changed by F_a for numerical stability, thus the method is an analogy of implicit method.) Here, τ is the relaxation time of T_s to T_b (time constant). Because the sub-skin layer is well mixed with the underlying layer under windy conditions, τ depends on the wind speed over the ocean. It is assumed that τ decreases exponentially as the wind speed increases, as in the following equation (see the equations in Gentemann et al., 2003, and Fig. 3a in Castro et al., 2003):

$$\tau = t_c\ exp(-U/U_e), \tag{3.43}$$

where t_c is the time constant when the wind speed is zero, U is the wind speed, and U_e is the wind speed when τ becomes $1/e$. Because the typical target timescale of the temperature variation is shorter than a day (e.g., diurnal cycle), t_c is set to 24 hours ($T_s > T_b$). However, it is empirically known that the sub-skin layer tends to mix with the underlying layer because of unstable stratification when the sub-skin layer temperature is lower than the temperature of the underlying layer ($T_s < T_b$); thus, t_c is set to a value shorter than 24 hours when $T_s > T_b$. Since the observed skin temperature declines at night (e.g., Castro et al., 2003) by one-fourth to one-sixth, t_c is set to one-fifth of the daytime temperature. It is assumed that the relaxation time is 1 hour when $T_s > T_b$ and 12 minutes when $T_s < T_b$ at a wind speed of 10 m/s, so U_e is set to 3.15 (= 10/log24). This assumption (i.e., $1/\ U_e = 0.32$) is practical because the wind effect corresponding to $1/U_e$ has a value of 0.53 or 0.29 (Gentemann et al., 2003) or 0.27 (Castro et al., 2003).

3.7.2. Sea-ice surface

The sea-ice surface temperature is a prognostic variable even in a general AGCM, and its variation is calculated at the same time as the sensible and latent heat fluxes by the implicit method. The snow surface processes are calculated in the same way as those for snow on land when snow (either partial or full coverage) is on the sea ice. The roughness length is set to a constant (0.001 m). The other parameters are fundamentally the same as for the sea surface. The temperature at the bottom of the sea ice and the sea-ice thickness are set to constants during the calculation of fluxes, and are used as lower boundary conditions in the AGCM. They are input from the OGCM in the CGCM. The snow amount

(water equivalent) on sea ice is a prognostic variable in the AGCM, and input from the OGCM in the CGCM, like the temperature at the bottom of the sea ice and sea-ice thickness. The amount of snowfall and sublimation are output to the OGCM from the AGCM. When there are multiple categories for sea-ice thickness in a single grid, these values are calculated for each category.

Albedo on sea ice

The formulation of sea-ice surface albedo is fundamentally similar to that in the Los Alamos sea ice model CICE (Hunke and Lipscomb, 2001). Both the ice albedo and the snow albedo are estimated. The sea-ice surface albedo is determined as an average weighted by the snow cover percentage, which depends on the snow amount. However, the parameterization of Aoki and Tanaka (2008), who account for the albedo decline due to pollution by aerosol deposition, is applied to the estimation of snow albedo. Moreover, the effect of penetration of solar radiation on albedo is taken into account for both ice and snow for visible and near-infrared wavelengths, respectively.

3.8. River and lake model

3.8.1. GRiveT

GRiveT (Global River model using TRIP) is the river-flow component (Fig. 9) used in MRI-ESM1. The river channel is the Total River Integrated Pathway (TRIP, Oki and Sud, 1998), either the 1° × 1° or the 0.5° × 0.5° version. The land-surface model in MRI-AGCM3 calculates river runoff in all land grids, and all river runoffs are transported by GRiveT to the river mouths via the river channels. GRiveT also has a lake in each TRIP grid, which is connected to the lake-surface component in MRI-AGCM3.

The predicted variables in GRiveT are the water masses (W) of river (r) and lake (l) and their inertial energies (E). The equations governing the water masses are

$$dWr \,/\, dt = \Sigma Frr_{in} + \Sigma Flr_{in} - Frr_{out} - Frl + Ro_{land} \qquad (3.44)$$

$$dWl \,/\, dt = Frl - Flr_{out} + P_{lake} - E_{lake} \qquad (3.45)$$

$$Frr = a\,Wr\,(c\varDelta t \,/\, L) \qquad (3.46)$$

$$Frl = (1{-}a)\,\mathrm{Wr}\,(c\varDelta t \,/\, L) \qquad (3.47)$$

$$Flr = Frl + (Wl - Wl_{std})/\tau \qquad (3.48)$$

Here, Frl, Flr, and Frr are the water fluxes; Ro_{land} is the river runoff estimated by the land-surface component (area weighted average); P_{lake} and E_{lake} are precipitation and evaporation estimated by the

lake-surface component (area weighted average); c is the river flow velocity (global constant, 0.4 m s^{-1}); Δt is the time step; L is the distance between the center of the grid and that of the downstream grid; a is a global constant $= 0.5$; Wl_{std} is the standard water mass of each lake (the depth is a global constant; 10 m); and τ is the e-folding timescale of the lake water mass (global constant, $O(10$ days$)$).

The inertial energies (E) of river and lake are defined as $E = c_{water} W (T - T_{frez})$, where c_{water} is the specific heat constant of liquid water, T is the temperature, and T_{frez} is 273.15 K (freezing point). El is also affected by the downward heat flux at the lake surface.
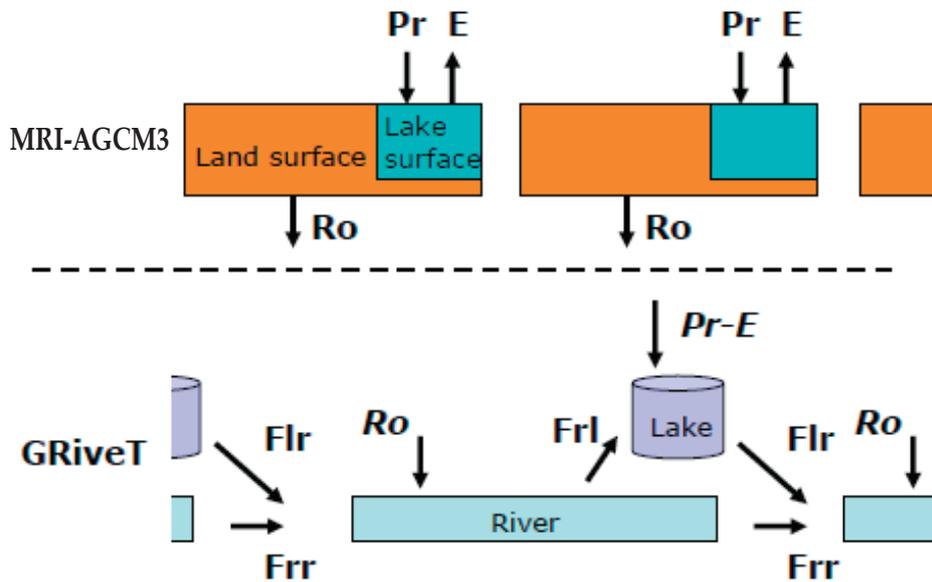

Figure 9   Schematics diagram of the river and lake model GRiveT